Mantle flow below the central and greater Alpine region: insights from SKS anisotropy analysis at AlpArray and permanent stations

Laura Petrescu[1,2], Silvia Pondrelli[1], Simone Salimbeni[1], Manuele Faccenda[3] and AlpArray Working Group*

5   [1]Istituto Nazionale di Geofisica e Vulcanologia, Bologna, Italy; [2]National Institute for Earth Physics, Bucharest, Romania; [3]University of Padua, Department of Geoscience, Padua, Italy; *For further information regarding the team, please visit the link which appears at the end of the paper.

Correspondence to: Silvia Pondrelli (silvia.pondrelli@ingv.it)

Abstract. The Alpine chain in western and central Europe is a complex orogen developed as a result of the African-Adriatic plate convergence towards the European continent and the closure of several Tethys oceanic branches. Seismic tomography studies detected high-wavespeed slabs plunging beneath the orogen to variable depths and a potential change in subduction polarity beneath the Central Alps. Alpine subduction is expected to leave a significant imprint on the surrounding mantle fabrics, although deformation associated with the Hercynian Orogeny which affected Europe prior to the collision with Adria may have also been preserved in the European lithosphere. Here we estimate SKS anisotropy beneath the central and greater Alpine region at 113 broadband seismic stations from the AlpArray experiment as well as permanent networks from Italy, Switzerland, Austria, Germany, and France. We compare the new improved dataset with previous studies of anisotropy, mantle tomography, lithospheric thickness, and absolute plate motion, and carry out Fresnel analysis to place constraints on the depth and origin of anisotropy. Most SKS directions parallel the orogen strike and the orientation of the Alpine slabs, rotating clockwise from west to east along the chain, from -45° to 90° over a ∼700 km distance. No significant changes are recorded in Central Alps at the location of the putative switch in subduction polarity, although a change in direction variability suggests simple asthenospheric flow or coupled deformation in the Central Swiss Alps transitions into more complex structures beneath the Eastern Alps. SKS fast axes follow the trend of high seismic anomalies across the Alpine Front, far from the present-day boundary, suggesting slabs act as flow-barriers to the ambient mantle surrounding them for hundreds of km. Further north across the foreland, SKS fast axes parallel Hercynian geological structures and are orthogonal to the Rhine Graben and crustal extension. However, large splitting delay times (>1.4s) are incompatible with a purely lithospheric contribution, but rather represent asthenospheric flow not related to past deformational events. West of the Rhine Graben, in northeastern France, anisotropy directions are spatially variable in the proximity of a strong positive seismic anomaly in the upper mantle, perhaps perturbing the flow-field guided by the nearby Alpine slabs.

1 Introduction

The Alpine tectonic region is a complex orogenic system formed as a result of the interaction between Africa and Europe throughout the Cenozoic era. The northward convergence of Adria led to the closure of several Tethys oceanic branches generating the arcuate Alpine-Dinaride-Carpathian orogenic system and the circum-Alpine rifts in Central and Western Europe (Figure 1, Schmid et al., 2004; Handy et al., 2010). While several geologic and geophysical studies suggest that Adria is the upper plate beneath the Western and Central Alps (the latter considered here to include Switzerland, westernmost Austria and Northern Italy), the origin of the eastern Alpine slab is the subject of ongoing debate. Several tomography studies show seismically fast subducted bodies down to 250-300 km beneath the Alps (e.g. Lippitsch et al., 2003; Piromallo and Morelli, 2003; Giacomuzzi et al., 2011; Zhu et al., 2015; Zhao et al., 2016), but their geometry, extent and orientation remain controversial (e.g. Lippitsch et al., 2003; Mitterbauer et al., 2011; Piromallo and Faccenna, 2004), with some studies further suggesting that the subduction direction changes polarity beneath the Central to Eastern Alps (e.g. Lippitsch et al., 2003; Schmid et al., 2004; Handy et al., 2015).

The collision between Adria and Europe is thought to have caused orogen-parallel asthenospheric flow (Barruol et al., 2011; Bokelmann et al., 2013; Salimbeni et al., 2018) and extrusion of the Eastern Alps towards the Pannonian Basin (Kummerow

45   et al., 2006; Bokelmann et al., 2013). In the Eastern Alps, Qorbani et al. (2015) also suggested that mantle flows above a deeper detached slab. Anisotropy studies in the Mediterranean suggested toroidal flow is likely induced by subducting and/or retreating slabs (e.g. Civello and Margheriti, 2004; Lucente et al., 2006; Baccheschi et al., 2007; Salimbeni et al., 2008; Buontempo et al., 2008; Diaz et al., 2010) and that trench-normal directions in the back-arc side may reorient to trench-parallel on the other side of the slab (Margheriti et al., 2003). While stations located in the high-topography Western Alps are

50   likely in correspondence of a forearc setting (Barruol et al., 2011), the uncertain origin and extent of the slab in the Eastern Alps (Lippitsch et al., 2003; Piromallo and Faccenna, 2004; Mitterbauer et al., 2011; Zhao et al., 2016) may place the stations in a hinterland setting, changing the way mantle flow can be interpreted with respect to the plunging Alpine slab. North of the Alpine Front, the European lithosphere which has been shaped by pre-Alpine Hercynian orogeny, experienced lithospheric thermal thinning due to Cenozoic rifting and possible mantle plume activity (e.g. Goes et al., 1999; Dèzes et al.,

55   2004). It is thus uncertain how far north and northwest collision-related asthenospheric flow may be extrapolated below the European foreland. Significant debate exists concerning the nature of the observed seismic anisotropy, with interpretations ranging from frozen-in pre-Hercynian paleo-subduction systems (Babuška and Plomerová, 2001), lithospheric deformation imprinted by the opening of the Rhine Graben (Walther et al., 2013), to a combination of basal drag due to plate motion and lithosphere-asthenosphere boundary topography influencing the mantle flow beneath (Bormann et al., 1996).

60   With the advent of the AlpArray project (Hetényi et al., 2018), seismic station density significantly increased in Europe, providing an unparalleled wealth of seismic data and excellent opportunity to probe the continental interior in the greater Alpine tectonic area. To help determine the past and present plate deformation and place constraints on the geodynamic controversies concerning slab geometries and the extent of collision-related asthenospheric flow, we determine upper mantle seismic anisotropy using SKS splitting analysis at both permanent and AlpArray seismic stations located across the Po Basin, the

65   Central and Eastern Alps, the Rhine Graben, and the Molasse Basin (Figure 2). SKS are core-refracted shear waves radiated by distant earthquakes that split in the presence of anisotropy, generally associated with strain-induced mineral alignment in the lithosphere and asthenosphere (Savage, 1999; Fouch and Rondenay, 2006; Long and Becker, 2010). SKS analysis thus yields direct observations of azimuthal anisotropy in the upper mantle, offering the possibility to passively probe the deformation of continents and mantle geodynamics (Silver, 1996). The broad and uniform coverage of the new AlpArray network

70   allows mapping the anisotropy with unprecedented density, providing fundamental insights on the distribution of deformation in the upper mantle.

2 Tectonic and geodynamic setting

The geological history of the Alps and the Mediterranean includes the sequential opening and closure of multiple Tethys and neo-Tethys oceanic branches throughout the Mesozoic, whose remnants were obducted on the southern margin of Europe

75   (Figure 1). After the collision between Adria and Europe started 35 Ma ago, the Adria indenter fuelled by the continued northward push of Africa rotated counter-clockwise with respect to Europe, thrusting over Europe towards W-NE (Coward and Dietrich, 1989, Froitzheim et al., 2008; Handy et al., 2010). Slab break-off was initiated, although time estimates vary between studies: 35–25 Ma (e.g. Piromallo and Faccenna, 2004) to 32–30 Ma (Sinclair, 1997) and may have migrated laterally, beneath the Eastern Alps and further into the Carpathians before 20 Ma (Ustaszewski et al., 2008) .

80   Geographically, the Alps comprise the Eastern Alps, lithologically linked to the Adria passive continental margin, and the Western Alps, comprising European terrains and ophiolite-bearing nappes. The Southern Alps, the northern continental margin of Adria unaffected by Alpine metamorphism, are separated from the Central and Eastern Alps by the EW oriented Insubric Fault, marking the suture between Adria and Europe, and the Periadriatic Fault (Figure 1) which accommodated shortening between Adria and Europe and post-collisional orogen-parallel extension (e.g. Schmid et al., 1989; Rosenberg et al.,

85   2015). In this paper, we refer to the Central Alps as the approximate region comprising the limit between the Western and Eastern Alps in Switzerland, west Austria and Northern Italy (Figure 1). Two major syn-orogenic basins flank the north and south of the Alpine orogen: the northern Molasse Basin, a typical foreland sedimentary basin, and the Po Basin to the south, also a foreland basin for the Apennines (Allen et al., 1986). To the north of the Alpine chain, the European foreland comprises terranes assembled during the pre-Alpine Hercynian Orogeny (280-380 Ma) along the EW trending Saxothuringian-

90   Moldanubian suture zone (Figure 1). The interaction between Africa and Eurasia caused the development of a synorogenic intra-continental foreland rift system which cross-cuts Hercynian paleo-boundaries (Ziegler, 1992). This system includes the Rhine Graben, an Eocene-Oligocene passive rift that may have been generated along preexisting planes of weakness in response to the Alpine and Pyrenean collisional phases (Schumacher, 2002; Dèzes et al., 2004). During the Miocene, the European foreland lithosphere suffered thermal weakening due to the activation of a mantle plume system beneath western and

95   central Europe, coeval with the Northeast Atlantic plumes (e.g. Goes et al., 1999; Ritter et al., 2001).

Tomographic images of the upper mantle structure beneath the Alpine region generally show slow seismic anomalies beneath part of the Western Alps (WA), the Molasse Basin (MB), and the eastern Po Basin. Fast seismic anomalies generally associated with the Alpine slab (Figure 1) are present beneath the western Po Basin, the Southern Alps (SA), and the Eastern Alps (EA) (e.g. Lippitsch et al., 2003; Piromallo and Morelli, 2003; Giacomuzzi et al., 2011; Zhu et al., 2015; Zhao et al.,

100   2016).The outline and internal properties of these anomalies are variable between studies, casting doubt on their lateral and depth extent, dipping direction or even whether they are continuous beneath the Alps. Although the general consensus regards the fast anomaly beneath the Western Alps as a south-southeastward subducted oceanic margin of Europe, the eastern segment may dip slightly towards the north and may be attached to Adria (Lippitsch et al., 2003; Handy et al., 2015). Furthermore, while the high seismic wavespeed Alpine "root" is present down to 250-300 km depth, at least beneath the West-

105   ern Alps (Piromallo and Faccenna, 2004, Zhao et al., 2016), a deeper slab, possibly the remnant Alpine Tethys (Figure 1), extends down to the bottom of the transition zone beneath the Eastern Alps (Piromallo and Faccenna, 2004; Mitterbauer et al., 2011).

3 Methods and data

SKS waves are excellent tools to study the anisotropy of the upper mantle beneath individual stations (e.g. Savage, 1999;
110 Long et al., 2017). They are S waves excited by distant earthquake that refracted through the Earth's outer core as P waves
and re-converted to S waves upon entering the mantle. When entering an anisotropic medium, SKS splits into two orthogo-
nally polarized waves that propagate at different speeds. The direction of the fast wave, φ, is generally parallel to the az-
imuthal anisotropy axis and the time delay, δt, can suggest the depth and/or strength of the anisotropy. Since anisotropy is
thought to be weak in the lower mantle (Niu and Perez, 2004) and in the transition zone (e.g. Tommasi et al., 2004), SKS
115 waves are generally associated with upper mantle anisotropy, thought to be induced by the alignment of olivine crystals in
the maximum strain direction(Ribe, 1989; Savage, 1999; Mainprice et al., 2000).

When SKS splitting occurs, energy is present on both radial and tangential components of the seismogram, resulting in an el-
liptical particle motion (Figure 3). If no energy is present on the tangential, the particle motion is linear and the SKS splitting
measurement is declared null (e.g. Wüstefeld and Bokelmann, 2007; Long and Silver, 2009). Several situations can result in
120 a null SKS split, the presence of multiple anisotropic layers whose combined signal destructively interferes (e.g. Barruol and
Hoffmann, 1999) or the azimuth of the incoming SKS wave corresponds to the anisotropy orientation or to a direction per-
pendicular to it. To determine the φ and dt parameters, we rotated the horizontal seismogram components in the great circle
arc reference frame and linearised the particle motion in the window encompassing the SKS arrival (Figure 3), by minimiz-
ing the energy on the tangential component (Silver and Chan, 1991). To avoid spurious results potentially introduced by low-
125 er mantle anomalies (Restivo and Helffrich, 2006), we only kept measurements where the difference between the source po-
larization of the SKS phase and its back-azimuth was found less than 20°.

We used data from 113 permanent and temporary seismic stations, including 65 stations from the temporary AlpArray net-
work (Hetenyi et al., 2018), operational since 2015, and 48 stations from multiple permanent networks (Figure 2): 6 stations
from Province Sudtirol Network (SI), 6 Italian National Seismic Network stations (IV), 20 Swiss Seismological Network sta-
130 tions (CH), 8 German Regional Seismic Network stations (GR) and 8 French National Seismic Network stations (FR). We
selected 542 earthquakes that occurred between 2015 and 2019, with magnitudes Mw > 5.8 and epicentral distances in the
range of 85°-130°, recorded at 113 broadband seismic stations (Figure 2). Data were filtered with a zero-phase Butterworth
bandpass filter between 0.04 Hz and 0.3 Hz and were manually selected for further analysis. After initial inspection of raw
three-component seismograms and post-analysis splitting quality control, we obtained between 3 and 35 viable solutions per
135 station, including null measurements (see Table 2SM, in Supplementary Material). Average SKS directions were computed
using the standard circular mean of fast axis back-azimuth angles and average delay time using standard linear mean. How-
ever, since this technique may not work well in cases when single-station circular distributions are too scattered, we also car-
ry out misfit surface stacking from individual non-null SKS splitting solutions, weighted by their signal to noise ratio (Resti-
vo and Hellfrich 1999). Since high back-azimuthal variations may yield high differences between the two averages (see Ta-
140 ble 3SM, in Supplementary Material), we compare them to assess single-station measurements heterogeneity (Figure 3).

4 Results

In Figure 4 all measurements are shown (see Supplementary Material, Table 1SM and 2SM). Most of the SKS fast axes follow a general NE-SW trend, especially those located in the higher Alpine elevation region (Figure 4a). In the Western Alps and north of the Alpine Front (within the Molasse Basin) some N-S directions are also recorded. In the Southern Alps and

145 Eastern Alps, anisotropy measurements progressively orient along an E-W direction, following a large-scale clockwise rotation of the fast axes along the chain. North of the Alpine Front, the Rhine Graben marks the transition between two different data distributions: the NE-SW observations in Germany change to a E-W average on the western side, in France. Here, measurements are more spatially heterogeneous: neighbouring stations record φ axes almost 90° different (Figure 4a). South of the Alpine Chain, in the Po Basin, SKS directions differ between west and east: fast axes display dominantly N-S orienta-

150 tions in the western part of the basin, where the doubly-verging Adriatic slabs meet the European slab. East of ∼10° longitude, φ directions become more scattered around the main NE-SW direction and tend to parallel the present-day plate boundary (Figure 1). Delay time distributions do not have a particular pattern: higher values are located in the French part of the Western Alps and in South Germany but also in the transition between Western-Central Alps and the Po Basin. Local areas with *dt* lower than 2 s are present in Central Germany at the Moldanubian-Saxothuringian transition and parts of the Po

155 Basin.

Null measurements provide additional valuable information on the nature and distribution of anisotropy beneath the Alps. Figure 4b shows the percentage value from the total number of viable SKS measurements at each station, as well as the direction of the incoming null SKS waves and their back-azimuthal coverage. Generally, stations with a small percentage of null measurements also yielded a large number of high-quality results and are mostly located in the Western Alps, Central

160 Alps in their upper front, and the eastern Po Basin. Stations with a higher null percentage (between 50 to 100%) are located in northern Switzerland (southwestern Molasse Basin) and in Central Germany, at the Moldanubian-Saxothuringian contact. At lower latitude (south and southeast of the Alpine Front) the amount of nulls decreases to lower than 50%. The Alpine Front also marks a change in the dominant direction of the un-split SKS waves coming from the SW and NE in the northern region and dominantly NW south of the Front. Events coming from N or E generally yield less null measurements (Figure 4b

165 inset).

Distributions of φ directions with respect to the back-azimuth of their corresponding earthquake also reveal a few emerging patterns across the region (Figure 4c). Most teleseismic events come from the SW and NE quadrants, yielding the most high-quality results in the western and central part of the study region. Projecting SKS fast axes at their 150 km piercing point depth would be expected to offset contrasting directions, if anisotropy was distributed laterally. However, in the French part

170 of the Western Alps and west of the Rhine Graben, large single-station φ variations belong to events coming from the same quadrant. In the Central Alps and part of Central Germany, directions are more laterally coherent, closely following the NE-SW trend, irrespective of the event back-azimuth. The N-S φ distribution is a secondary trend emerging in the Molasse Basin

and is yielded by events coming from the SW (Figure 4c). A smaller subset of SE and NW events are better recorded in the Eastern Alps but yield scattered φ directions, including NE-SW, E-W, and NW-SE.

175 To better visualise the distribution of fast axes with respect to the event back-azimuth for stations located in different geographical positions, we plot examples of three representative high-quality station data (Figure 4d). Station A061A, located in the Central Swiss Alps, yields a homogeneous φ distribution over the entire event back-azimuthal range, resulting in a small difference between the average circular value and the value obtained by misfit surface stacking (Figure 4d). Station A037A is located at the transition between the Central and the Eastern Alps, in western Austria and yields a bimodal φ distribution

180 along a dominant NE-SW axis and a secondary E-W direction. In this case a more evident difference in the mean values indicates a greater dispersion in the results. Station A300A, representative for the eastern Po Basin, yields high-quality measurements from events in the 45–100° and 250–310° back-azimuthal range, with the most frequent φ along NE-SW. The average value calculated from circular statistics is different from that calculated with the stacking procedure, supporting an emerging trend of anisotropy heterogeneity towards the eastern part of the network.

185 Trends visualised in maps are even more evident in sections. Results from this study are averaged along with measurements from previous studies in 50 km by 50 km, along- and off-plane distances, respectively. Variations of splitting parameters in the section quasi-parallel to the Alpine Chain confirm the large-scale clockwise rotation of φ axes from west to east , from -45° to 90° over a ∼700 km distance (Figure 5, section D). Sections perpendicular to the Alpine Chain indicate more variability in φ and *dt*. Section A crosses the Alps from SE to NW, starting from the northern termination of the Apennines,

190 where φ directions are ∼ -30° and *dt* ranges between 1-2.5s. Across the western Po Basin two distinct distributions emerge, yielding a similar mean φ value to the Apennines and variable *dt* values. In the Southern and Central Alps, separated by the Insubric Fault (Figure 1), φ directions are more homogenous, following the main NE-SW direction and *dt* is between 0.5-1.5 s. Across the European-Alpine Front and the Molasse Basin, φ axes rotate from ∼50° to ∼30° and *dt* increases above 1.5 s. Stations in the Jura Mountains have more dispersed φ values averaging around 45° and *dt* between 1-2 s and measurements

195 become strongly scattered beneath the European Foreland in France. Sections B and C are both perpendicular to the Alpine Chain, crossing the Po Basin, Southern and Central Alps, the Molasse Basin into Southern Germany. A common feature is that the distribution of fast axes is more coherent when entering the European foreland (EF) from the south, where the average value stabilises around 45° (section B) and ∼60° (section C). The onset of homogeneity, however, starts below the Central Alps in section B, while further east along section C, the Periadriatic Fault (Figure 1) marks the transition from complex

200 anisotropy to simple coherent measurements. In section C, φ in the European Foreland rotates from ∼60° beneath the Molasse Basin to almost 90° in South Germany, across the Moldanubian and Saxothuringian terranes (Figure 5).

5. Discussion

5.1 Comparison with previous SKS-splitting studies

205 Our measurements of φ and dt are generally coherent, similar in magnitude and direction with previous studies of SKS an-isotropy at neighbouring stations and provide a smooth spatial continuity in the previously irregular measurement coverage (Figures 5 and 6a). The average clockwise rotation of φ directions from the Western to the Central Alps are in agreement with results from Salimbeni et al. (2018) and Barruol et al. (2011), although more significant single station heterogeneity is displayed by stations located in the French Western Alps, implying more complex anisotropic structure in the deformed fore-

210 land European lithosphere than measurements in the Swiss Central Alps. Around 10° longitude, the secondary E-W trending φ pattern becomes more evident in the Central-Eastern Alps transition, as also noticed by Bokelmann et al. (2013) and Qorbani et al. (2015), although a more abrupt change was considered to occur at ~13°, across the Tauren window in Austria. The ENE-SSW average measurements are also in agreement with the studies of Kummerow et al. (2006) and Bokelmann et al. (2013).

215 In the eastern Alpine region, in Austria and NE Italy, more heterogeneous φ directions (Figure 4) are similar to previous measurements (Salimbeni et al., 2013; Qorbani et al., 2015), where multilayer modelling suggested an interference between eastward directed flow above a deeper detached Tethyan slab with intrinsic anisotropy (Qorbani et al., 2015). A secondary E-W fast anisotropy trend is also present in the eastern Southern Alps and the eastern Po Basin, similar to measurements of Salimbeni et al. (2013), who suggested that the juxtaposition of the Alpine and Dinaric mantle deformational fields may play

220 a role in the detected φ variations.

North of the Alpine Front, in the Molasse Basin and in the underlying Hercynian-aged Saxothuringian-Moldanubian struc-tures, our measurements are generally consistent both in φ direction and delay times with the SKS parameters estimated at permanent and temporary stations in Germany (Bormann et al., 1996; Plenefisch et al., 2001; Walther et al., 2013). While the ESE-WNE direction is dominant, a progressive change in φ directions across the Molasse Basin and the underlying

225 Saxothuringian-Moldanubian terranes, evident especially in section C (Figure 5), has also been pointed out by Plenefisch et al. (2001). Some stations in the Saxothuringian-Moldanubian transition yielded only null measurements (Figure 5), and a secondary N-S trend also develops in the Molasse Basin, similar to one station analysed near the Rhine Graben by Walther et al. (2013).

5.2 Depth and source of SKS anisotropy in the Alpine region

230 A first-order indication of the depth of anisotropy or the path of the anisotropic SKS phase is the splitting delay time. The continental crust typically accounts for only 0.1-0.3 s (Silver, 1996) or 0.1-0.5 s (Barruol and Mainprice, 1993) contribution to the observed SKS splitting delay, which are incomparably smaller than our δt values with a mean of 1.4 s, requiring a mantle contribution. Furthermore, we can estimate the thickness of an anisotropic layer using the average dt as $L = dt \times \beta / k$

(Silver and Chan, 1988; Helffrich, 1995), where β is the shear velocity (4.48 km/s in the upper mantle Kennett et al., 1995)

235   and k is the average anisotropy percentage (4% average in the upper 200km, Savage, 1999), yielding ~160 km of possible anisotropic path length. This estimate exceeds the crustal or even lithospheric depths proposed in the Alps (between 80 and 110 km, Miller and Agostinetti, 2012; Geissler et al., 2010; Bianchi et al., 2014), suggesting that the SKS signal may either represent asthenospheric flow beneath the orogen, or it is a combination of lithospheric deformation and underlying mantle flow.

240   Most collisional orogenic systems are characterised by anisotropy that aligns with the structural grain of the belt and has of-ten been considered to reflect asthenospheric flow due to collision (e.g. Meissner et al., 2002) or a signature of combined as-thenospheric origin and vertically coherent deformation within the lithosphere (Wang et al., 2008; Chang et al., 2015; Kuo et al., 2018). To better constrain the depth and eventually the vertical coherency of the anisotropy sampled by SKS, we com-pare our measurements with the direction of the anisotropy described by the Pn phase (Diaz et al., 2012), which propagates

245   along the Moho interface and is indicative of subcrustal anisotropic properties (Figure 6). SKS fast axis directions are some-where similar to Pn anisotropy in the Central (Swiss) Alps, Southern and Eastern Alps, and partially in the Molasse Basin, but disagree quite completely with it north of ~48° latitude and in northeast France. In addition, an ambient noise study of azimuthal anisotropy in the Swiss Alps (Fry et al., 2010), detected a change in anisotropy orientation from orogen-parallel within the crust to orogen-perpendicular directions at lower crustal depths. If the equivalent anisotropic layer thickness is

250   ~160 km and lithospheric thickness is ~80 km in the area, at least part of the SKS anisotropic path must reside in the litho-sphere. However, at least in the Central (Swiss) Alpine region, the lack of back azimuthal variation in SKS observations at single stations (Figure 4) is not consistent with multiple layers of anisotropy, but rather indicative of simple asthenospheric flow or/and a coupled lithosphere-asthenosphere deformation, with an unchanged anisotropy with depth.

The approximate source depth of anisotropy can also be estimated by evaluating the possible overlap of SKS Fresnel zones

255   at a certain range of depths (Alsina and Snieder, 1995). The radius of the Fresnel zone Rf, can be estimated from the main period of the SKS phase, T, the S-wave velocity v at depth h, and the angle of incidence θ as Rf = sqrt[(Tvh/2cos(θ)] (e.g. Pearce and Mittleman, 2002; Margheriti et al., 2003). The depth at which Fresnel zones of SKS phases coming from oppo-site directions overlap is usually interpreted to show an upper bound for the anisotropy source. Figure 6b shows examples of Fresnel zones for three AlpArray stations that show anomalous SKS observations with respect to the surrounding stations.

260   Fresnel analysis at both stations shows that Fresnel zones for two opposite SKS waves intersect at least down to ~200 km, suggesting that different anisotropic sources must reside below this depth. At station A288A, in the Southern Alps, south of the Insubric Fault, the geological suture between Europe and Adria, Fresnel zones at 200 km still partially overlap, suggest-ing an even deeper source in this region. Here, estimates of the LAB depth show a lithospheric thickness of ~140 km (Miller and Agostinetti, 2012) at the approximate location of A288A. In contrast, LAB depths at the station A037A are shallower,

265   with estimates between 70-90 km (Bianchi et al., 2014) and 100-120 km (Geissler et al., 2010). In both sites we can infer a lateral variation in the anisotropy pattern below LAB.

5.3 Comparison with tomography: relationships with slabs and circum-Alpine seismic anomalies

To understand how deeper upper-mantle structure may be connected with SKS observations, we also test for correspondence
between our measurements and 3D seismic heterogeneities (Figure 7). A high-Vp anomaly, often interpreted as the south-
270 ward plunging European slab, lies beneath the Alpine chain obliquely (Figure 1), extending under the western Po-Basin,
Southern, Central, and Eastern Alps, down to ~300 km (Lippitsch et al., 2003; Piromallo and Morelli, 2003; Giacomuzzi et
al., 2011; Zhu et al., 2015; Zhao et al., 2016). Stations in the Western Alps, part of the Central Alps, and the Molasse Basin
are underlain by negative Vp anomalies and are usually interpreted to be located on the fore-arc side of the southward plung-
ing European slab. SKS parallel the trend of the positive anomaly and do not seem to change directions across its boundaries.
275 We chose to interpret our observations in relation to the most recent seismic tomography of Europe (Zhu et al., 2015), espe-
cially because the model incorporates azimuthal anisotropy parameters. Purely isotropic velocity models are prone to con-
tamination with artefact anomalies, where anisotropy has not been taken into account (e.g. Bezada et al., 2016).

Surveys of crustal structure and upper-mantle tomography images of the Alpine chain led to a different interpretation for the
origin of the Alpine slab beneath the Eastern Alps, suggesting that a lithospheric fragment lithologically linked to the Adria
280 plate dips northward beneath the eastern section of the orogen (Lippitsch et al., 2003; Handy et al., 2015). A switch in sub-
duction polarity is thus expected at the transition between the Western and Eastern Alps, around 10°-11°E. However, there is
no marked change in SKS anisotropy at that longitude, except for a progressive clockwise reorientation of the SKS axes
(Figure 5), which broadly follow the orogenic trend and parallel the strike of the positive seismic velocity anomalies. The
secondary E-W φ distribution (Figure 4) appears at stations located east of 10° longitude, at the border between Switzerland,
285 Austria, and NE Italy. Bokelmann et al. (2013) also identifies a change in SKS directions although the onset of this trend is
placed more eastward, across the Tauern window, where the Adriatic indenter is known to act towards the N-NE (Bus et al.,
2009), actively causing tectonic escape of the Eastern Alpine units (Kummerow et al., 2006). While SKS patterns are not
sufficient evidence to support a hypothetical switch in subduction polarity at 10-11°, the subtle change in single station indi-
vidual SKS φ patterns imply a change in mantle deformation styles at this longitude, either due to escape mechanisms or the
290 influence of a more complex slab structure beneath.

In the western Po Basin, multiple positive seismic velocity anomalies coalesce (Figure 7), likely the signature of the complex
interaction between the subducted northwestern segment of Adria and the southeastward plunging European lithosphere.
Here, measurements are more heterogeneous (Figure 4), probably indicating complex flow patterns due to the presence of
multiple subductions. φ directions show a transition from the typical central Alpine NE-SW trend towards a N-S orientation
295 that continues into the Apennines (Figure 5). In the eastern Po Basin, low negative seismic anomalies, coupled with high
subsidence rates and isostasy imbalance estimates, pointed out a possible asthenospheric downwelling mechanism (Faccenna
et al., 2014). However, vertical movement of mantle material would have a significant effect on SKS measurements (e.g.
Xue and Allen, 2005; Levin et al., 2018, Petrescu et al. 2020). Vertically-oriented deformation in the upper mantle would be
transparent to the nearly vertical propagation path of SKS phases, whose particle motion samples the horizontal azimuthal

300   anisotropy. Our SKS measurements in the eastern Po Basin are especially devoid of null-measurements (Figure 4b) and thus do not support this hypothesis, but it is worth to note that further south Salimbeni et al. (2008) found an increasing amount of null measurements that could be indicative of a downwelling mechanism.

5.4 Extent of asthenospheric flow in response to collision north of the Alpine Front

Most SKS observations from the high-topography region south of the Alpine Front are interpreted as collision-related as-
305   thenospheric flow (Barruol et al., 2011; Bokelmann et al., 2013; Qorbani et al., 2015). While this explanation may be justi-fied in a region of recent orogenic activity, the similarity between SKS measurements north of the Alpine Front and those south of it (Figure 5) beg the question whether anisotropy beneath stable Europe is still related to the Alpine orogeny and the vertically plun

ging slabs act as flow-barriers. North and northwest of the Alpine Front, the European lithosphere suffered pre-Alpine defor-
310   mation during the Hercynian Orogeny with remnant sutures trending along an approximate WSW-ENE direction (Figure 1). The most recent phases of extension affecting the Rhine Graben follow the same orientation as the Hercynian surface geo-logic trends (e.g. Schumacher, 2002), raising the possibility that anisotropy measurements here also record more recent litho-spheric extension, as also proposed by Walther et al. (2013).

North of the Alpine Front, our measured SKS fast axis directions parallel both surface geological structures (Figure 4) and
315   absolute plate motion direction in a no-net rotation frame (25.68 mm/yr speed, 50° azimuth from N, Kreemer et al., 2014) and are perpendicular to maximum horizontal stress (oriented mostly NNW-SSE, Heidbach et al., 2018). However, LAB depths beneath the Molasse Basin are too shallow (80-100 km, Geissler et al., 2010) compared to the anisotropic layer thick-ness estimated from delay times (∼170 km) to justify a purely lithospheric contribution to the observed anisotropy. Fresnel arguments support that the strongest anisotropy may be located below ~200 km depth, where it varies laterally. The slow
320   speed plate motion may be insufficient to induce coherent basal drag mineral fabrics (Debayle and Ricard, 2013), so we can discard the influence of absolute plate movement as well. Moreover, the crustal contribution is too small to be taken into consideration (Barruol and Mainprice, 1993) and the discrepancy between Pn anisotropy mostly sensitive to lower-crustal and sub-Moho depth ranges and our SKS measurements (Figure 6) further supports a deeper source for the latter. Therefore anisotropy beneath the circum-Alpine region has a clear sub-lithospheric contribution and most probably reflects the effect
325   of Alpine collision, suggesting the presence of vertical slabs beneath the Alps control asthenospheric flow for a few hundred km beneath the European foreland. The change in SKS fast polarisations across the Alpine Front is, however, more signifi-cant further west in Profile A (Figure 5), where homogeneously distributed anisotropy observations in the Swiss Alps switch into the less coherent directions estimated at stations west of the Rhine Graben (Figure 4). Up to 90° φ changes occur in the proximity of a fast seismic anomaly that develops in north-east France (Figure 7). This upper-mantle anomaly, possibly a
330   remnant Hercynian lithospheric root, may be affecting the surrounding flow, interacting with the barrier flow-field created by the Alpine slabs.

Further north in central Germany, across the Moldanubian-Saxothuringian boundary, average SKS directions rotate clock-wise by ∼40° (Figure 5, profile C). Plenefisch et al. (2001) also observed a rotation in fast axes across the Moldanubian to Saxothuringian terranes, interpreting it as an evidence that their boundary extends to lithospheric depths. At this distance,

335   SKS observations can partially contain a lithospheric paleo-deformational signature (e.g. Babǔska and Plomerová, 2006). However, LAB depths here are ∼100-120 km (Geissler et al., 2010; Plomerová and Babǔska, 2010), indicating a 60-80 km mantle lithosphere, assuming an average crustal thickness of 40 km. This is still too small to account for the observed split-ting delay times (Figure 4), suggesting SKS anisotropy has a clear asthenospheric contribution, perhaps not related to Alpine or Hercynian deformation. As Bormann et al. (1996) also pointed out, seismically estimated temperatures at lithospheric

340   depths may be too high to allow the development and long-time preservation of fossil anisotropy. The European lithosphere suffered thermal thinning due to Cenozoic rifting and possible mantle plume activity connected to the Atlantic plume system (e.g. Goes et al., 1999; Dèzes et al., 2004), whose far-field influence may start to be manifested here.

6 Conclusions

To place constraints on the mantle deformation beneath the Central Alps and the greater Alpine region, we analyse SKS

345   splitting at 113 new broadband seismic stations belonging to the AlpArray seismic experiment and permanent stations in Italy, Austria, Switzerland, France, and Germany. SKS directions are mostly parallel to the orogenic strike and the trend of the subducted slabs beneath the Alpine Chain, rotating clockwise from -45° to 90° from west to east. Splitting delay times average to ∼1.4 s and are mainly representative of active asthenospheric flow around the plunging Alpine slabs. There is no large scale change in SKS directions or delay times at the location of a putative subduction polarity switch beneath the Cen-

350   tral Alps, although we note a certain subtle change in anisotropy complexity. Simple flow or a coupled lithosphere-astheno-sphere deformation may dominate the mantle beneath the Central Swiss Alps, where directions follow a consistent NE-SW trend, while more complex structures develop beneath the Eastern Alps, in agreement with previous studies on this region and further east. In the Po Basin SKS directions differ between west and east: fast axes have prevailing N-S orientations in the western part beneath which opposite Adriatic flanks meet the European slab. East of ∼10° longitude, SKS directions be-

355   come more scattered around the main NE-SW trend and do not support a presumed asthenospheric downwelling related to the subduction of Adria. North of the Alpine Front, orogen-parallel anisotropy persists, implying that the effect of the Alpine slabs acting as flow-barriers extends far beneath the foreland. At the contact between the Moldanubian and Saxothuringian terranes, sutured during the Hercynian Orogeny, directions experience an almost 40° rotation. However, the thin lithosphere beneath the region is insufficient to account for the observed splitting delay time. Therefore, we interpret anisotropy there as

360   asthenospheric and that may start to feel the influence of mantle processes unrelated to past Hercynian deformation, crustal extension, or the indentation of Adria. To the west of the Rhine Graben, in northeast France, a strong positive seismic anom-

aly is located at upper-mantle depths and SKS anisotropy measurements are highly variable in its proximity, suggesting a lo-
350 cal perturbation in the flow-field in the greater Alpine region.

Team list

The complete member list of the AlpArray Working Group can be found at http://www.alparray.ethz.ch.

Acknowledgments

355 LP was supported by the European Research Council project Newton Grant agreement 758199, under H2020-EU.1.1. The
complete member list of the AlpArray Working Group can be found at http://www.alparray.ethz.ch. Data from permanent
stations used in this study were obtained from multiple network archives: the Italian National Seismic Network
(https://doi.org/10.13127/SD/X0FXnH7QfY), the Swiss Seismological Network (https://doi.org/10.12686/sed/networks/ch),
the German Regional Seismic Network (https://doi.org/10.25928/mbx6-hr74), the French National Seismic Network
360 (https://doi.org/10.15778/RESIF.FR), and the Province Sudtirol Seismic Network (SI,
http://cnt.rm.ingv.it/en/instruments/network/SI). Most figures were made using GMT software (Wessel and Smith, 1998).

Supplementary Material

Tables of original measurements and average values discussed in this paper are included as Table1SM for no-null
measurements, Table2SM for null measurements and Table3SM Average values.

365 **References**

Allen, P.A., P., Homewood, and G.D., Williams, (1986), Foreland basins: An introduction, in Allen, P.A., and Homewood,
P., eds., Foreland basins: Inter- national Association of Sedimentologists Special Publication 8, p. 3-12.
Alsina, D., and R. Snieder (1995), Small-scale sublithospheric mantle deformation: constraints from SKS splitting observa-
tions., Geophys. J. Int., 123, 431–448.
370 Babǔska V., and J., Plomerová (2006) European mantle lithosphere assembled from rigid microplates with inherited seismic
anisotropy. Phys Earth Planet Inter 158: 264-280, http://doi.org/10.1016/j.pepi.2006.01.010.
Baccheschi, P., L. Margheriti, and M. Steckler (2007), Seismic anisotropy reveals focused mantle flow around the Calabrian
slab (Southern Italy), Geophys. Res. Lett., 34(5), doi: 10.1029/2006GL028899.
Barruol, G., and R. Hoffmann (1999), Upper mantle anisotropy beneath the Geoscope stations, J. Geophys. Res., 104(B5),
375 10,757–10.
Barruol, G., and D. Mainprice (1993), A quantitative evaluation of the contribution of crustal rocks to the shear-wave split-
ting of teleseismic SKS waves., Phys. Earth Planet. Int., 78, 281–300.

Barruol, G., M. Bonnin, H. Pedersen, G. H. Bokelmann, and C. Tiberi (2011), Belt-parallel mantle flow beneath a halted continental collision: The Western Alps, Earth Planet. Sci. Lett., 302(3-4), 429–438, doi:10.1016/j.epsl.2010.12.040.

380   Bezada, M., M. Faccenda, and D. Toomey (2016), Representing anisotropic subduction zones with isotropic velocity models: A characterization of the problem and some steps on a possible path forward, Geochem. Geophys. Geosyst., 17 (8), 3164–3189, doi:10.1002/2016GC006507.

Bianchi, I., M. S. Miller, and G. Bokelmann (2014), Insights on the upper mantle beneath the Eastern Alps, Earth and planetary science letters, 403, 199–209, doi: 10.1016/j.epsl.2014.06.051.

385   Bokelmann, G., E. Qorbani, and I. Bianchi (2013), Seismic anisotropy and large-scale deformation of the Eastern Alps, Earth Planet. Sci. Lett., 383, 1–6, doi:10.1016/j.epsl.2013.09.019.

Bormann, P., G. Grünthal, R. Kind, and H. Montag (1996), Upper mantle anisotropy beneath central Europe from SKS wave splitting: effects of absolute plate motion and lithosphere-asthenosphere boundary topography?, J. Geodyn., 22(1-2), 11–32, doi: 10.1016/0264-3707(96)00014-2.

390   Buontempo, L., G. Bokelmann, G. Barruol, and J. Morales (2008), Seismic anisotropy beneath southern Iberia from SKS splitting, Earth Planet. Sci. Lett., 273(3-4), 237–250, doi: 10.1016/j.epsl.2008.06.024.

Bus, Z., G. Grenerczy, L. Táoth, and P. Máonus (2009), Active crustal deformation in two seismogenic zones of the Pannonian region—GPS versus seismological observations, Tectonophysics, 474, 343–352, doi:10.1016/j.tecto.2009.02.045.

Chang, L., L. M. Flesch, C.-Y. Wang, and Z. Ding (2015), Vertical coherence of deformation in lithosphere in the eastern

395   Himalayan syntaxis using GPS, Quaternary fault slip rates, and shear wave splitting data, Geophys. Res. Lett., 42(14), 5813–5819, doi: 10.1002/2015GL064568.

Civello, S., and L. Margheriti, (2004), Toroidal mantle flow around the Calabrian slab (Italy) from SKS splitting, Geophys. Res. Lett., 31 (10), doi:10.1029/2004GL019607.

Coward, M., and D. Dietrich (1989), Alpine tectonic overview, Geological Society, London, Special Publications, 45(1), 1–

400   29, doi:10.1144/GSL.SP.1989.045.01.01.

Debayle, E., and Y. Ricard, (2013), Seismic observations of large-scale deformation at the bottom of fast-moving plates, Earth. Planet. Sci. Letters, http://dx.doi.org/10.1016/j.epsl.2013.06.025.

Dèzes, P., S. Schmid, and P. Ziegler (2004), Evolution of the European Cenozoic Rift System: interaction of the Alpine and Pyrenean orogens with their foreland lithosphere, Tectonophysics, 389(1-2), 1–33, doi:10.1016/j.tecto.2004.06.011.

405   Diaz, J., J. Gallart, A. Villasenõr, F. Mancilla, A. Pazos, D. Córdoba, J. Pulgar, P. Ibarra, and M. Harnafi (2010), Mantle dynamics beneath the Gibraltar Arc (western Mediterranean) from shear-wave splitting measurements on a dense seismic array, Geophys. Res. Lett., 37 (18), doi:10.1029/2010GL044201.

Diaz, J., A. Gil, and J. Gallart (2012), Uppermost mantle seismic velocity and anisotropy in the Euro-Mediterranean region from Pn and Sn tomography, Geophys. J. Int., 192 (1), 310–325, doi:10.1093/gji/ggs016.

410   Faccenna, C., T. W. Becker, M. S. Miller, E. Serpelloni, and S. D. Willett (2014), Isostasy, dynamic topography, and the elevation of the Apennines of Italy, Earth Planet. Sci. Lett., 407, 163–174.

Fouch, M. J., and S. Rondenay (2006), Seismic anisotropy beneath stable continental interiors, Phys. Earth Planet. Int., 158(2), 292–320, doi:10.1016/j.pepi.2006.03.024.

Froitzheim, N., D. Plăsienka, and R. Schuster (2008), Alpine tectonics of the Alps and Western Carpathians, The Geology of
415 Central Europe, 2, 1141–1232.

Fry, B., F. Deschamps, E. Kissling, L. Stehly, and D. Giardini (2010), Layered azimuthal anisotropy of Rayleigh wave phase velocities in the European Alpine lithosphere inferred from ambient noise, Earth Planet. Sci. Lett., 297 (1-2), 95–102, doi:10.1016/j.epsl.2010.06.008.

Geissler, W. H., F. Sodoudi, and R. Kind (2010), Thickness of the central and eastern European lithosphere as seen by S re-
420 ceiver functions, Geophys. J. Int., 181(2), 604–634, doi: 10.1111/j.1365-246X.2010.04548.x.

Giacomuzzi, G., C. Chiarabba, and P. De Gori (2011), Linking the Alps and Apennines subduction systems: new constraints revealed by high-resolution teleseismic tomography, Earth Planet. Sci. Lett., 301(3-4), 531–543, doi:10.1016/j.epsl.2010.11.033.

Goes, S., W. Spakman, and H. Bijwaard (1999), A lower mantle source for central European volcanism, Science, 286(5446),
425 1928–1931, doi:10.1126/science.286.5446.1928.

Handy, M. R., S. M. Schmid, R. Bousquet, E. Kissling, and D. Bernoulli (2010), Reconciling plate-tectonic reconstructions of Alpine Tethys with the geological–geophysical record of spreading and subduction in the Alps, Earth-Science Reviews, 102(3-4), 121–158, doi: 10.1016/j.earscirev.2010.06.002.

Handy, M. R., K. Ustaszewski, and E. Kissling (2015), Reconstructing the Alps–Carpathians–Dinarides as a key to under-
430 standing switches in subduction polarity, slab gaps and surface motion, Int. J. of Earth Sci., 104 (1), 1–26, doi:10.1007/s00531-014-1060-3.

Heidbach, O., M. Rajabi, X. Cui, K. Fuchs, B. Müller, J. Reinecker, et al (2018), The World Stress Map database release 2016: crustal stress pattern across scales. Tectonophys., 744:484–498, https://doi.org/10.1016/j.tecto.2018.07.007.

Helffrich, G. (1995), Lithospheric deformation inferred from teleseismic shear wave splitting observations in the United
435 Kingdom, J. Geophys. Res., 100 (B9), 18,195–18,204.

Hetényi, G., I. Molinari, J. Clinton, G. Bokelmann, I. Bondár, W. C. Crawford, J.-X. Dessa, C. Doubre, W. Friederich, F. Fuchs, et al. (2018), The AlpArray Seismic Network: A large scale European experiment to image the Alpine orogen, Surveys in Geophysics, 39(5), 1009–1033, doi:10.1007/s10712-018-9472-4.

Kennett, B. L. N., E. R. Engdahl, and R. Buland (1995), Constraints on seismic velocities in the earth from traveltimes, Geo-
440 phys. J. Int., 122, 108–124.

Kreemer, C., G. Blewitt, and E. C. Klein (2014), A geodetic plate motion and Global Strain Rate Model, Geochem. Geophys. Geosyst., 15, doi:10.1002/ 2014GC005407.

Kummerow, J., R. Kind, T. W. Group, et al. (2006), Shear wave splitting in the Eastern Alps observed at the TRANSALP network, Tectonophysics, 414(1-4), 117–125, doi: 10.1016/j.tecto.2005.10.023.

445   Kuo, B.-Y., S.-C. Lin, and Y.-W. Lin (2018), SKS splitting and the scale of vertical coherence of the Taiwan mountain belt, J. Geophys. Res., 123(2), 1366–1380, doi:10.1002/2017JB014803.

Levin, V., M. D. Long, P. Skryzalin, Y. Li, and I. López (2018), Seismic evidence for a recently formed mantle upwelling beneath New England, Geology, 46(1), 87–90.

Lippitsch, R., E. Kissling, and J. Ansorge (2003), Upper mantle structure beneath the Alpine orogen from high–resolution

450   teleseismic tomography, J. Geophys. Res., 108 (B8), doi: 10.1029/2002JB002016.

Long, M., and P. Silver (2009), Shear Wave Splitting and Mantle Anisotropy: Measurements, Interpretations, and New Directions, Surveys in Geophysics, 30(4), 407–461, doi: 10.1007/s10712-009-9075-1.

Long, M. D., and T. W. Becker (2010), Mantle dynamics and seismic anisotropy, Earth Planet. Sci. Lett., 297(3), 341–354, doi:10.1016/j.epsl.2010.06.036.

455   Long, M. D., H. A. Ford, L. Abrahams, and E. A. Wirth (2017), The seismic signature of lithospheric deformation beneath eastern North America due to Grenville and Appalachian orogenesis, Lithosphere, 9(6), 987–1001, doi:10.1130/L660.1.

Lucente, F. P., L. Margheriti, C. Piromallo, and G. Barruol (2006), Seismic anisotropy reveals the long route of the slab through the western-central Mediterranean mantle, Earth Planet. Sci. Lett., 241(3-4), 517–529, doi:10.1016/j.epsl.2005.10.041.

460   Mainprice, D., G. Barruol, and W. B. Ismail (2000), The seismic anisotropy of the Earth's mantle: from single crystal to polycrystal, Earth's Deep Interior: Mineral physics and tomography from the atomic to the global scale, 117, 237–264, doi:10.1029/GM117p0237.

Margheriti, L., F. Lucente, and S. Pondrelli (2003), SKS splitting measurements in the Apenninic-Tyrrhenian domain (Italy) and their relation with lithospheric subduction and mantle convection, J. Geophys. Res., 108 (B4), doi:10.1029/

465   2002JB001793.

Meissner, R., W. D. Mooney, and I. Artemieva (2002), Seismic anisotropy and mantle creep in young orogens, Geophys. J. Int., 149 (1), 1–14, doi:10.1046/j.1365-246X.2002.01628.x.

Miller, M. S., and N. P. Agostinetti (2012), Insights into the evolution of the Italian lithospheric structure from S receiver function analysis, Earth Planet. Sci. Lett., 345, 49–59.

470   Mitterbauer, U., M. Behm, E. Brückl, R. Lippitsch, A. Guterch, G. R. Keller, E. Koslovskaya, E.-M. Rumpfhuber, and F. Sŭmanovac (2011), Shape and origin of the East-Alpine slab constrained by the ALPASS teleseismic model, Tectonophysics, 510(1-2), 195–206, doi: 10.1016/j.tecto.2011.07.001.

Niu, F., and A. M. Perez (2004), Seismic anisotropy in the lower mantle: A comparison of wave- form splitting of SKS and SKKS, Geophys. Res. Lett., 31 (24), doi:10.1029/2004GL021196.

475   Petrescu, L., G. Stuart, G. Houseman, and I. Bastow (2020), Upper mantle deformation signatures of craton-orogen interaction in the Carpathian-Pannonian region from SKS anisotropy analysis, Geophys. J. Int., doi:10.1093/gji/ggz573.

Pearce, J., and D., Mittleman, (2002), Defining the Fresnel zone for broadband radiation, Phys. Rev. E, 66(5), 056602, doi:10.1103/PhysRevE.66.056602.

Piromallo, C., and C. Faccenna (2004), How deep can we find the traces of Alpine subduction?, Geophys. Res. Lett., 31(6), doi:10.1029/2003GL019288.

Piromallo, C., and A. Morelli (2003), P wave tomography of the mantle under the Alpine- Mediterranean area, J. Geophys. Res., 108 (B2), doi:10.1029/2002JB001757.

Plenefisch, T., S. Faber, K.-P., Bonjer, (1994). Investigations of Sn and Pn phases in the area of the upper Rhine Graben and northern Switzerland, Geophys. J. Int., 119, 402-420.

Plomerová, J., and Babuška, V. (2010). Long memory of mantle lithosphere fabric—European LAB constrained from seismic anisotropy, Lithos, 120(1), 131–143.

Qorbani, E., I. Bianchi, and G. Bokelmann (2015), Slab detachment under the Eastern Alps seen by seismic anisotropy, Earth Planet. Sci. Lett., 409, 96–108, doi:10.1016/j.epsl.2014.10.049.

Qorbani, E., G. Bokelmann, I. Kovács, F. Horváth, and G. Falus (2016), Deformation in the asthenospheric mantle beneath the Carpathian-Pannonian Region, J. Geophys. Res., 121 (9), 6644–6657, doi:10.1002/2015JB012604.

Restivo, A., and G. Helfrich (1999), Teleseismic shear wave splitting measurements in noisy environments. Geophys. J. Int. 137 (3), 821–830.

Restivo, A., and G. Helfrich (2006), Core-mantle boundary structure investigated using SKS and SKKS polarization anomalies, Geophys. J. Int., 165(1), 288–302.

Ribe, N. M. (1989), Seismic anisotropy and mantle flow, J. Geophys. Res., 94(B4), 4213–4223, doi:10.1029/JB094iB04p04213.

Ritter, J. R., M. Jordan, U. R. Christensen, and U. Achauer (2001), A mantle plume below the Eifel volcanic fields, Germany, Earth Planet. Sci. Lett., 186 (1), 7–14, doi:10.1016/S0012- 821X(01)00226-6.

Rosenberg, C. L., A. Berger, N. Bellahsen, and R. Bousquet (2015), Relating orogen width to shortening, erosion, and exhumation during Alpine collision, Tectonics, 34(6), 1306–1328, doi:10.1002/2014TC003736.

Salimbeni, S., S. Pondrelli, L. Margheriti, J. Park, and V. Levin (2008), SKS splitting measurements beneath Northern Apennines region: a case of oblique trench-retreat, Tectonophysics, 462(1-4), 68–82, doi:10.1016/j.tecto.2007.11.075.

Salimbeni, S., S. Pondrelli, and L. Margheriti (2013), Hints on the deformation penetration induced by subductions and collision processes: Seismic anisotropy beneath the Adria region (Central Mediterranean), J. Geophys. Res., 118 (11), 5814–5826, doi:10.1002/2013JB010253.

Salimbeni, S., M. G. Malusà, L. Zhao, S. Guillot, S. Pondrelli, L. Margheriti, A. Paul, S. Solarino, C. Aubert, T. Dumont, S. Schwartz, Q. Wang, X. Xu, T. Zheng and R. Zhu (2018), Active and fossil mantle flows in the western Alpine region unravelled by seismic anisotropy analysis and high-resolution P wave tomography, Tectonophysics, 731, 35–47, doi:10.1016/j.tecto.2018.03.002.

Savage, M. (1999), Seismic anisotropy and mantle deformation: What have we learned from shear wave splitting?, Rev. Geophys., 37, 65–106, doi:10.1029/98RG02075.

Schmid, S., H. Aebli, F. Heller, and A. Zingg (1989), The role of the Periadriatic Line in the tectonic evolution of the Alps, 45 (1), 153–171.

Schmid, S. M., B. Fügenschuh, E. Kissling, and R. Schuster (2004), Tectonic map and overall architecture of the Alpine orogen, Eclogae Geologicae Helvetiae, 97(1), 93–117, doi: 10.1007/s00015-004-1113-x.

Schmid, S. M., D. Bernoulli, B. Fügenschuh, L. Matenco, S. Schefer, R. Schuster, M. Tischler, and K. Ustaszewski (2008), The Alpine-Carpathian-Dinaridic orogenic system: correlation and evolution of tectonic units, Swiss J. Geosci., 101(1), 139–183, doi:10.1007/s00015-008- 1247-3.

Schumacher, M. E. (2002), Upper Rhine Graben: role of preexisting structures during rift evolution, Tectonics, 21(1), 6–1.

Silver, P., and G. Chan (1991), Shear wave splitting and subcontinental mantle deformation, J. Geophys. Res., 96(B10), 16,429–16,454, doi:10.1029/91JB00899.

Silver, P., and W. Chan (1988), Implications for continental structure and evolution from seismic anisotropy, Nature, 335(6185), 34–39.

Silver, P. G. (1996), Seismic anisotropy beneath the continents: Probing the depths of geology, Annu. Rev. Earth Planet. Sci., 24 (1), 385–432.

Sinclair, H.D., (1997), Tectonostratigraphic model for underfilled peripheral foreland basin: An Alpine perspective. Geol. Soc. Amer. Bull. 109, 3, 324-346.

Tommasi, A., M. Godard, G. Coromina, J. Dautria, and H. Barsczus (2004), Seismic anisotropy and compositionally induced velocity anomalies in the lithosphere above mantle plumes: a petrological and microstructural study of mantle xenoliths from French Polynesia, Earth Planet. Sci. Lett., 227(3), 539–556, doi:10.1016/j.epsl.2004.09.019.

K. Ustaszewski, S. Schmid, B. Fügenschuh, M. Tischler, E. Kissling, W. Spakman, (2008), A map-view restoration of the Alpine-Carpathian-Dinaridic system for the Early Miocene, Swiss J. Geosci., 101, 273-294.

Walther, M., T. Plenefisch, and G. Rümpker (2013), Automated analysis of SKS splitting to infer upper mantle anisotropy beneath Germany using more than 20 yr of GRSN and GRF data, Geophys. J. Int., 196(2), 1207–1236, doi:10.1093/gji/ggt456.

Wang, C.-Y., L. M. Flesch, P. G. Silver, L.-J. Chang, and W. W. Chan (2008), Evidence for mechanically coupled lithosphere in central Asia and resulting implications, Geology, 36(5), 363–366, doi:0.1130/G24450A.1.

Wessel, P., and H.F. Smith (1998). New, improved version of 538 the generic mapping tools released, Eos Trans AGU, 539, 79-579; doi:10.1029/98EO00426.

Wüstefeld, A., and G. Bokelmann (2007), Null detection in shear-wave splitting measurements, Bull. Seis. Soc. Am., 97(4), 1204.

Xue, M., and R. M. Allen (2005), Asthenospheric channeling of the Icelandic upwelling: Evidence from seismic anisotropy, Earth Planet. Sci. Lett., 235(1-2), 167–182, doi: 10.1016/j.epsl.2005.03.017.

Zhao, L., A. Paul, M. G. Malusà, X. Xu, T. Zheng, S. Solarino, S. Guillot, S. Schwartz, T. Dumont, S. Salimbeni, et al.
545 (2016), Continuity of the Alpine slab unraveled by high-resolution P wave tomography, J. Geophys. Res., 121 (12), 8720–
8737, doi:10.1002/2016JB013310.

Zhu, H., E. Bozdağ, and J. Tromp (2015), Seismic structure of the European upper mantle based on adjoint tomography,
Geophys. J. Int., 201(1), 18–52, doi:10.1093/gji/ggu492.

Ziegler, P. A. (1992), European Cenozoic rift system, Tectonophys., 208(1-3), 91–111, doi:10.1016/0040-1951(92)90338-7.
550
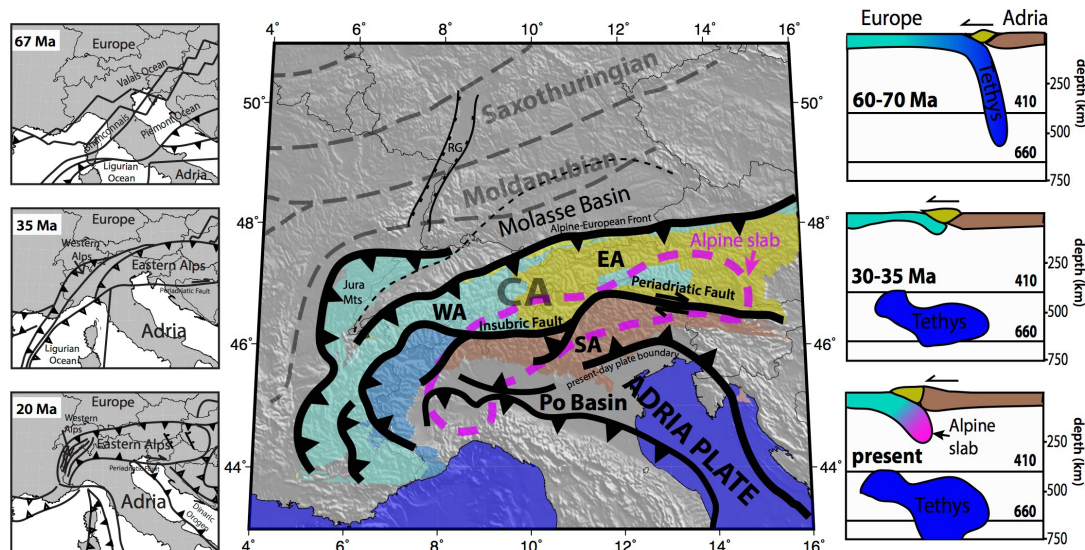
Figure 1: Geographical units of the Alpine Chain and surrounding regions. Coloured areas represent the main geological regions are based on Schmid et al. (2008) and mark the Eastern Alps (EA, yellow), the Southern Alps (SA, brown), and the Western Alps (WA, light and dark blue). TW: Tauern Window. Dashed pink line marks the probable outline of the Alpine slab, after Mitterbauer et al. (2011). Left: Plate tectonic reconstruction snapshots of the region for the past 67 Ma, according to Handy et al. (2010).
560 **Right: Time-lapse of probable trench migration and slab break-off beneath the Alps for the past 70 Ma, after Piromallo and Faccenna (2004). The section showing the Alpine slab (pink), attached to the European lithosphere (cyan), may only be applicable to the Western and Central Alps. In the Eastern Alps, the slab may be attached to Adria (yellow and brown).**

565
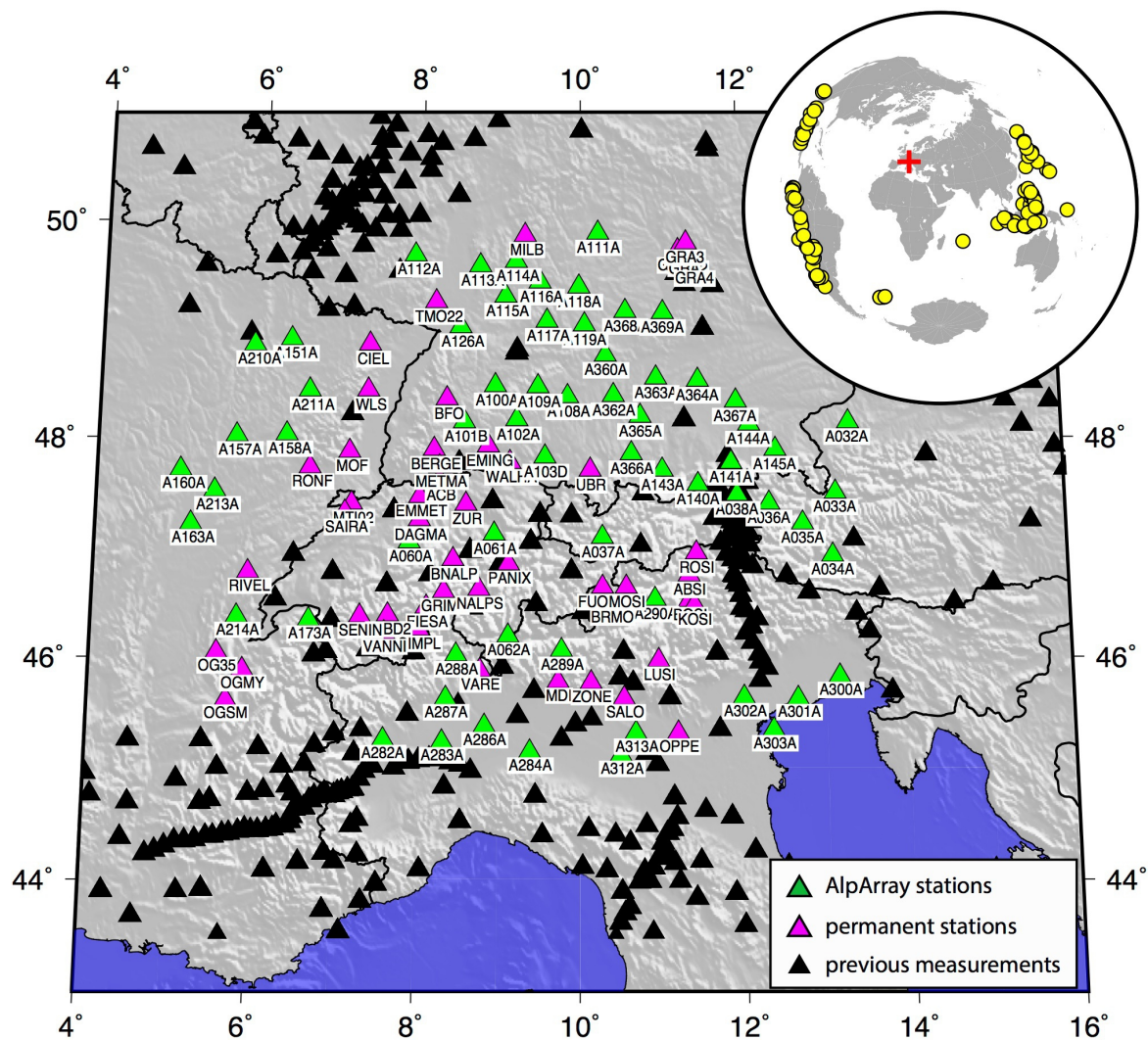
Figure 2: Topographic and political map of the central Alpine region showing broadband seismic stations (triangles) whose data were analysed in this study, including AlpArray temporary stations (green), permanent stations (magenta), and stations with previous SKS measurements (black). Inset shows the location of earthquakes used in this study (yellow circles) and the centre of our study area (red cross).

570
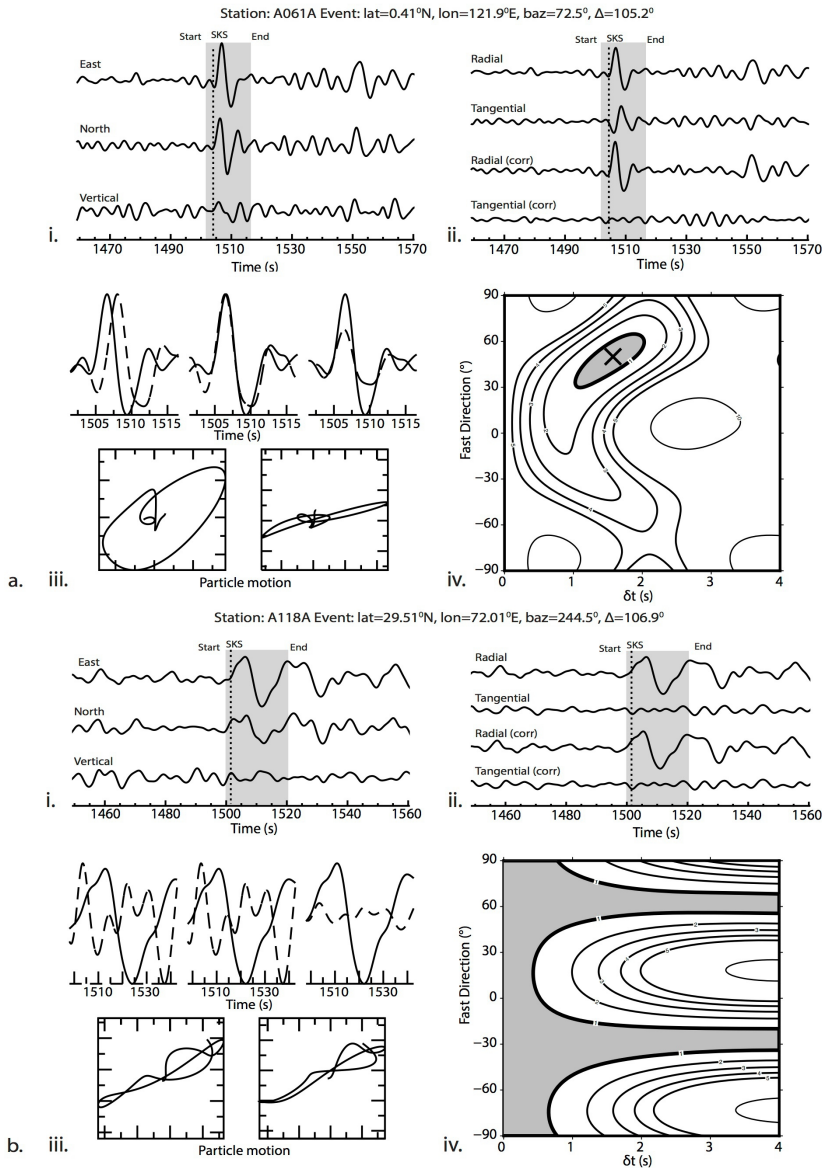
Figure 3: Examples of SKS analysis procedure for a successful SKS splitting measurement (a) and a situation where no energy is present on the tangential component, referred to as a null measurement (b). i. Three-component seismograms recorded at station A061A, with the region comprising the SKS phase highlighted. ii. The radial and tangential component seismograms, after rotation to the great circle arc (top two) and after the SKS splitting correction (bottom two). iii. Top: Windows of the SKS phase from the radial (black line) and tangential component (dashed line) before and after the correction. Bottom: Particle motion before and after correction. iv. Misfit contour surface showing the best solution pair of *dt* and φ (cross) and the 1-sigma uncertainty surface (highlighted region).
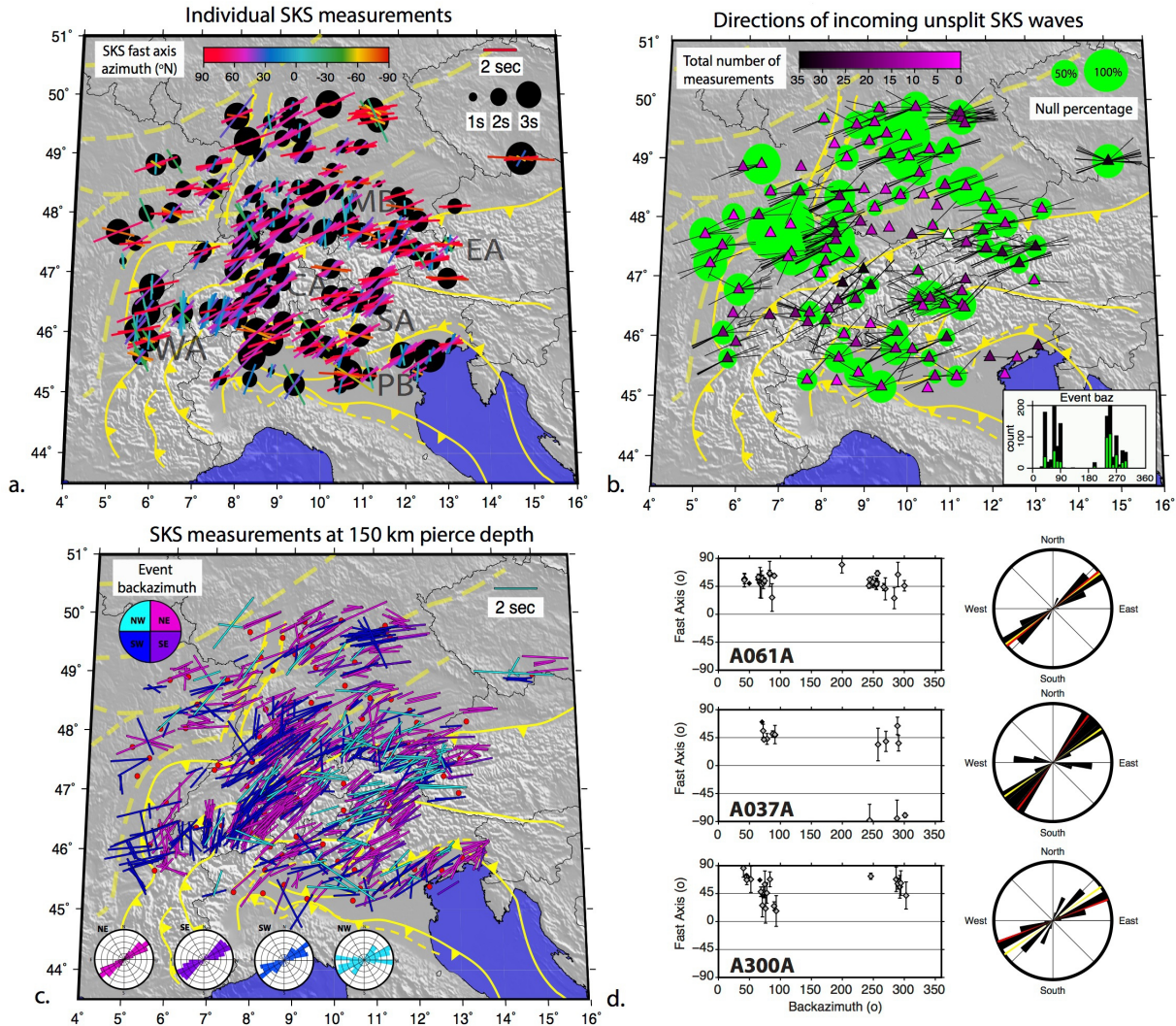
Figure 4: a) Map of individual SKS fast axis (bars) and time delay (black circles) measurements at seismic stations. Colours represent SKS fast axis back-azimuth. Yellow lines are major tectonic faults. Dashed yellow lines mark the limits of the Molasse and the Po sedimentary basins, respectively. **b)** Map of the Alpine region comprising the percentage of nulls (green circles) from the total number of measurements at each seismic station (coloured triangles). Bars indicate the direction of incoming SKS waves which yielded null measurements. Inset: histogram of high-quality earthquakes analysed in this study (black bars) and the number of nulls (green bars) in 10° back-azimuthal bins. **c)** SKS measurements (bars) coloured with respect to the back-azimuth and shifted to the 150 km piercing point. Rose diagrams represent polar histograms of the SKS fast axis directions, for earthquakes coming from the NW, NE, SW, and SE, respectively. **d)** Results at stations from different regions: A061A (Swiss Alps), A037A (Central Alps) and A300A (Eastern Po Basin). Left: Plots of the SKS fast axis measurements versus back-azimuth. Right: Normalised rose diagrams of SKS fast axis directions, average SKS direction computed using the circular average (yellow) and the the one obtained by stacking misfit surfaces from individual SKS splitting solution (red).
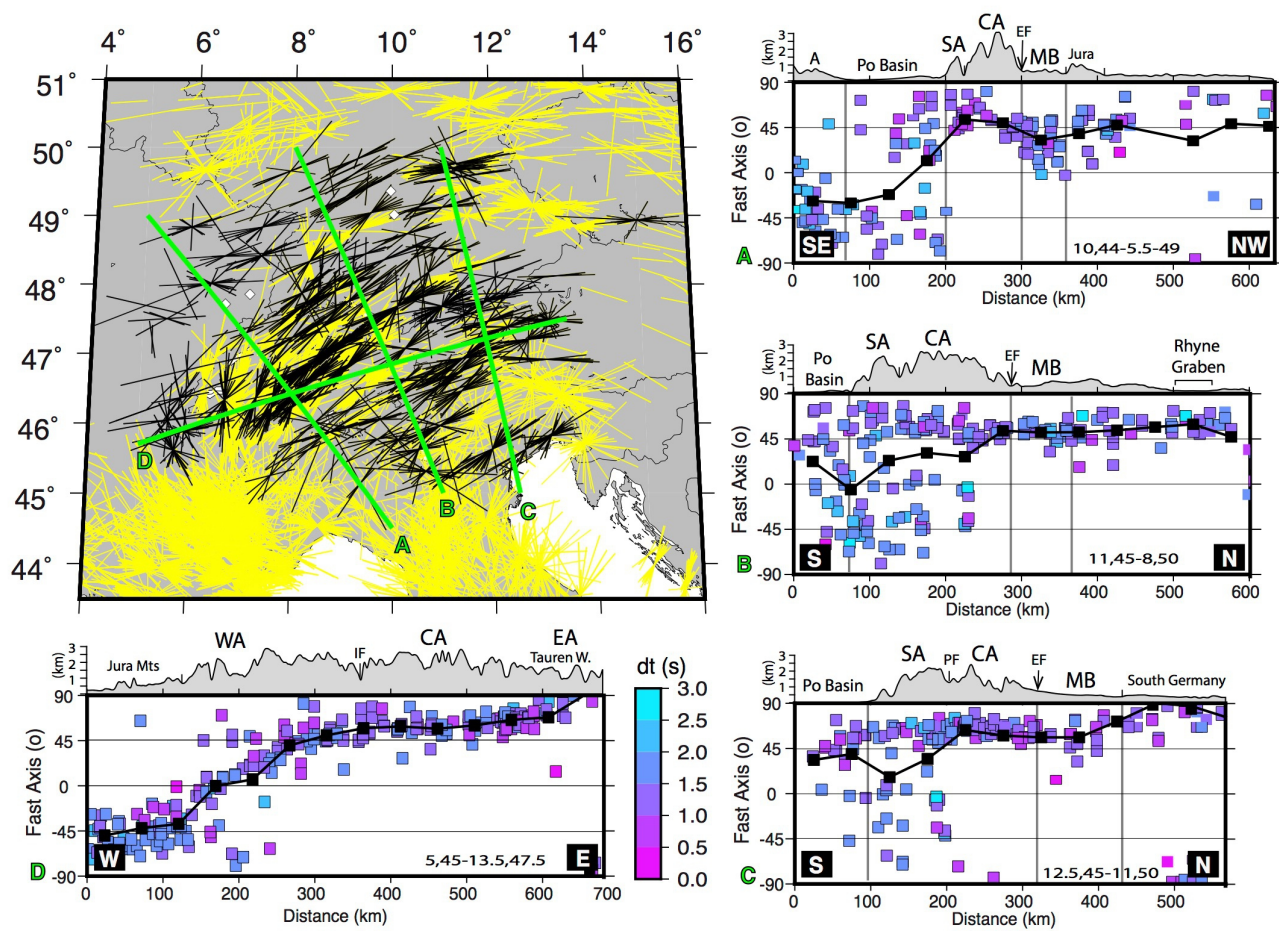
595

Figure 5: Sections of SKS splitting parameters across and along the Alpine orogen. Top right: Map of western and central Europe showing past SKS results (yellow lines) and observations from this study (black lines). The green lines mark the location of chosen sections. Left: Sections across the orogen showing average SKS fast axes direction variation for profiles A, B and C. On top of each section topography is reported and the location of major geological units: SA (Southern Alps), CA (Central Alps), WA (Western Alps), PF (Periadriatic Fault), IF (Insubric Fault), AF (Alpine Front). Black squares are average φ direction along the profile in 50 km distance intervals.

600
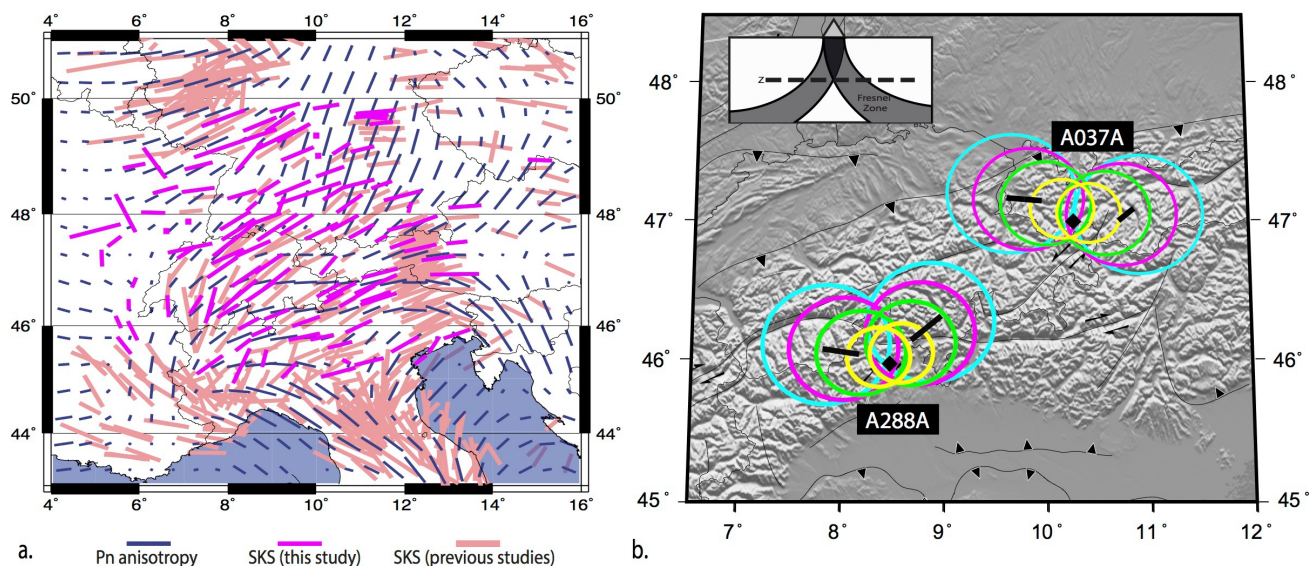
Figure 6: a. Comparison between our SKS measurements (red bars), Pn anisotropy axes, and previous SKS measurements (Diaz et al., 2012, and references therein). b. Single station Fresnel analysis of SKS observations at three AlpArray seismic stations from two earthquakes from opposing directions. Coloured circles show the approximate Fresnel zone for the SKS wave at different depths: 50 km (yellow), 100 km (green), 150 km (magenta), and 200 km (cyan). Black lines show the SKS fast axis direction projected at its 150 km piercing point. The inset is a cross-section of the Fresnel zones of two incoming SKS waves from opposing directions and the depth where these zones overlap (after Alsina and Snieder, 1995).
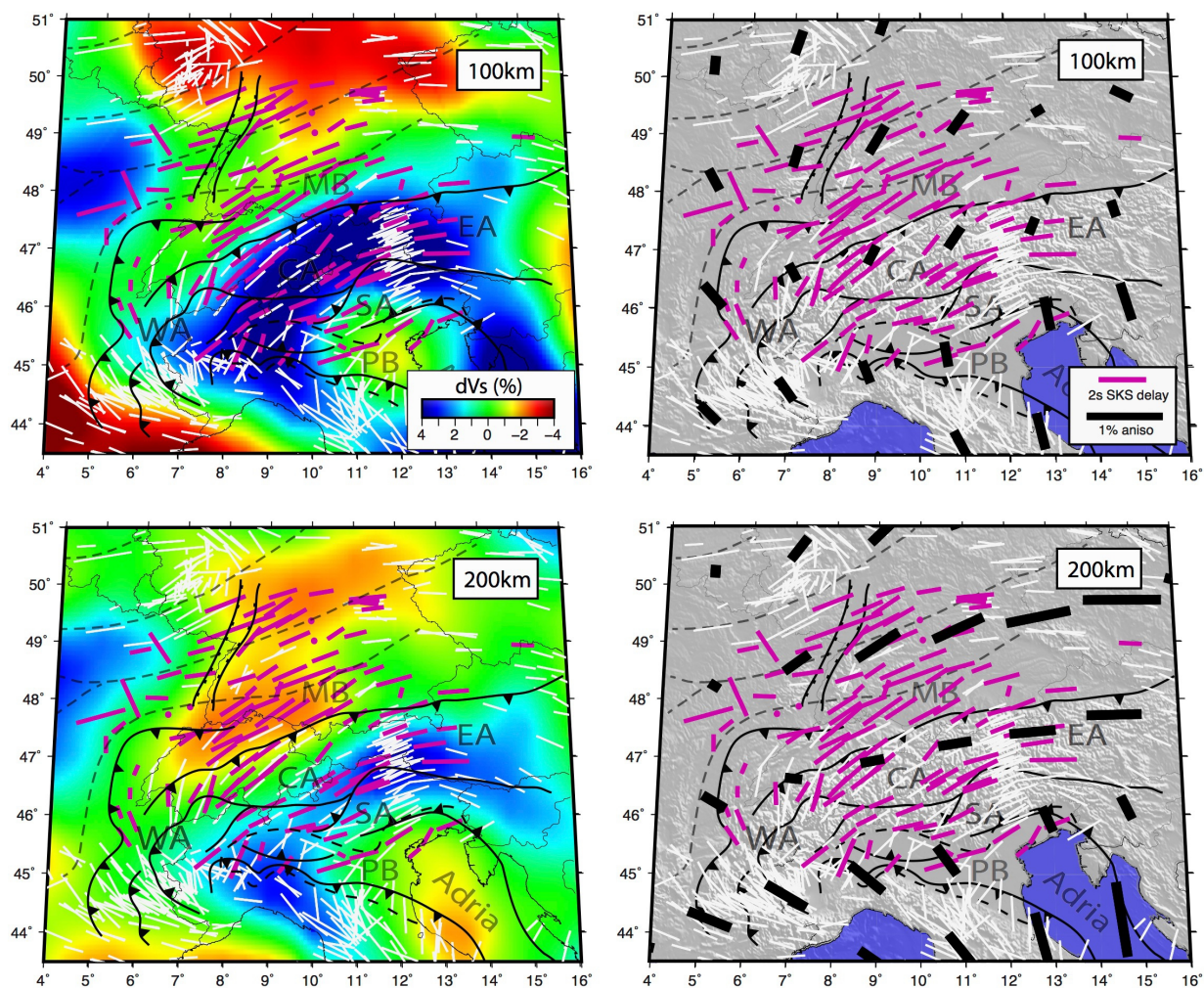
Figure 7: a. Comparison of SKS results with the seismic tomography model of Zhu et al. (2015) at 100 km and 200 km. Magenta lines are SKS fast axes and delay times obtained in this study, while white bars are previous measurements (Salimbeni et al., 2008, 2013; Barruol et al., 2011; Kummerow et al., 2006; Bokelmann et al., 2013; Qorbani et al., 2016). b. Comparison of SKS results from this study and previous measurements with azimuthal anisotropy percentages (black bars) estimated by Zhu et al. (2015) at 100 km and 200 km, respectively.